

H₂-Induced Pressure Broadening and Pressure Shift in the *P*-Branch of the ν_3 Band of CH₄ from 300 to 700 K

Ehsan Gharib-Nezhad¹, Alan N. Heays^{2,3}, Hans A. Bechtel⁴, James R. Lyons²

¹*School of Molecular Sciences, Arizona State University, Tempe, AZ. 85287, USA.*

²*School of Earth and Space Exploration, Arizona State University, Tempe, AZ. 85287, USA.*

³*NASA Astrobiology Institute, NASA Ames Research Center, Moffett Field, CA., USA.*

⁴*Advanced Light Source, Lawrence Berkeley National Laboratory, Berkeley, CA. 94720, USA.*

Abstract

For accurate modelling of observations of exoplanet atmospheres, quantification of the pressure broadening of infrared absorption lines for and by a variety of gases at elevated temperatures is needed. High-resolution high-temperature H₂-pressure-broadened spectra are recorded for the CH₄ ν_3 -band *P*-branch. Measured linewidths for 116 transitions between 2840 and 3000 cm⁻¹ with temperature and pressures ranging between 300 and 700 K, and 10 and 933 Torr, respectively, were used to find rotation- and tetrahedral-symmetry-dependent coefficients for pressure and temperature broadening and pressure-induced lineshifts. The new pressure-broadening data will be useful in radiative-transfer models for retrieving the properties of observed exoplanet atmospheres.

Keywords: Methane (CH₄), High-Temperature FTIR Spectroscopy, High-Temperature Pressure-induced collisional broadening and shift, Lorentzian linewidth coefficients, exoplanetary atmospheres, hydrogen-dominant atmospheres

1. Introduction

Methane (CH₄) has been observed in the infrared spectra of different solar-system atmospheres including those of terrestrial planets (e.g., on the surface of Mars [1, 2]), Jovian planets (e.g., Jupiter, Saturn, Uranus [3, 4]), and Titan [5, 6]. The abundance of CH₄ is also important in constraint understanding the C/O ratio in the atmospheres of brown dwarfs and exoplanets, as well as understanding their formation history [7, 8]. Because the thermochemically dominant carbon-bearing molecule at T > 1200 K is CO and at T < 800 K is CH₄ [6], their mixing ratios with CO₂ are used as a temperature probe and to determine super-Earths/sub-Neptune metallicities [9, 10]. Moreover, CH₄ near-infrared (NIR) spectra are an important tool for classifying brown dwarf types (e.g., T-dwarfs [11]). Despite extensive endeavors to model the

chemical composition of exoplanetary atmospheres by means of radiative transfer modeling (i.e., transmission and emission exoplanetary spectra [12–14]), a proposed detection of CH₄ is still under debate [15]. Additionally, high-resolution Earth-based searches of methane through the cross-correlation technique have been unsuccessful [16]. However, it has been argued thermochemically that CH₄ is one of the main absorbers in super-Earth to sub-Neptune atmospheres [17]. H₂ is the major broadening molecule (or perturber) in these exoplanetary atmospheres, and therefore, the accuracy of radiative transfer modeling, particularly for the cross-correlation technique (see section 3.5 in [18]), relies strongly upon the accuracy and completeness of CH₄ spectroscopic data including rovibrational transitions and pressure-broadening coefficients appropriate for high-temperature and H₂-dominated atmospheres [19, 20]. Accurate quantification

of pressure-broadening coefficients at room- and high-temperature is fundamental because they influence the absorption cross-section data and, therefore, the modeled exoplanet atmospheric spectra [20, 21].

Methane is a tetrahedral molecule with five symmetry species: A_1 , A_2 , E , F_1 , and F_2 . The ν_3 fundamental band arises from asymmetric C–H stretching (see chapter 7 in [22]). Given the relevance of CH₄ infrared (IR) absorption and emission in the study of brown dwarfs and planetary/exoplanetary atmospheres, many experimental and theoretical studies recorded or computed the relevant rovibrational transitions. High-resolution IR spectra of CH₄ have been recorded at both room [23, 24] and high temperatures [25–30]. Additionally, several ab-initio studies have computed the CH₄ rovibrational transitions [25, 31–34].

Since the 1980s, several laboratory measurements of the pressure-broadening of CH₄ by various broadeners (hereafter referred to as absorber@[broadener], e.g., CH₄@[H₂]) at room temperature have been made. Non-Voigt pressure-broadening coefficients of the CH₄@[H₂, N₂, Ar, or He] ν_3 band Q branch were analyzed using a laser spectrometer at high resolution [35, 36] and showed a strong dependency of linewidths on broadener and total angular-momentum quantum number, J . In addition, the measured linewidths are dependent on the tetrahedral symmetry species (i.e., A_1 , A_2 , E , F_1 , F_2). The R -branch of the $3\nu_3$ overtone (~ 9000 cm⁻¹) of CH₄@[H₂] was measured up to $J_{\text{lower}} = J''=6$ by Fourier transform spectroscopy with 0.01 cm⁻¹ spectral resolution [37, 38].

Several studies have used quantum or semi-classical approaches to calculate, predict, and explain pressure broadening of CH₄ in different broadeners (or perturbers)[39]. Anderson theory, for instance, utilizes a perturbation approach to compute the line broadening and their temperature-dependence coefficients through electrostatic interactions [40–42]. However, it was shown later that electrostatic forces are not able to explain the broadening for some perturbers such as O₂ and N₂ [43]. In comparison, Robert-Bonamy theory [44] was used to show the atom-atom potential energy is the main cause of collisional broadening for these species [45].

To the best of our knowledge, there are no measurements of CH₄@[H₂] (or any other broadeners) at $T > 315$ K. Measurements for temperatures between 200 and 300 K show the temperature-dependence coefficient (n_γ , see

section 4.2) of the ν_3 band of CH₄@[Air] and CH₄@[N₂] is 0.6 – 1.0 [46] and 0.94–0.97 [43], respectively. For the ν_4 band of CH₄@[Air] and CH₄@[N₂], n_γ is 0.5 – 0.8 [47]. A complete list of literature regarding measurement of temperature-dependence coefficients is reported in Table 5.

For this study, we used Fourier-transform infrared spectroscopy (FTIR) to record rovibrational lines of CH₄@[H₂] in the P branch of the ν_3 band over the temperature range 300–700 K (Sec. 2). Then, using a least-squares fitting analysis, the Lorentzian linewidth (γ_L) and temperature-dependence coefficients (n_γ) are determined for $J''=2-17$ (Sec. 3). The dependency of the Lorentzian coefficients on total quantum number J'' and the tetrahedral symmetry species is discussed in Sec. 4.

2. Experimental details

2.1. Instrumental setup

All spectra in this study were recorded with a Bruker 125HR infrared Fourier-transform spectrometer located at the Advanced Light Source (ALS) of the Lawrence Berkeley National Laboratory (LBNL). As shown in Fig. 1, the evacuated sample chamber in this model of spectrometer is located between the beam splitter and detector. In this case, the thermal IR emission from the heated sample gas cells does not contribute to the recorded interferogram, and no post-analysis correction for the cell emission is required in comparison with other studies in which the heated cell was placed at the entrance to the spectrometer (e.g., Ref. [26]). For measurements at high temperature, we designed a sealed monolithic gas cell. Due to its high transmittance over a spectral range of 2750–3250 cm⁻¹ and high melting point, the whole gas cell and spectral windows are fabricated from fused quartz.

2.2. Recorded Spectra

We recorded spectra for temperatures 300, 500 and 700 K and over a pressure range of $\sim 0.8 - 7.0$ Torr for CH₄ gas and $\sim 10 - 933$ Torr (0.013–1.2 atm) of H₂ broadening gas. In total, four quartz gas cells with a path length of 10 ± 0.2 cm were used in these measurements. Different amounts of CH₄ and H₂ gases were inserted in each tube at room temperature and then the port was

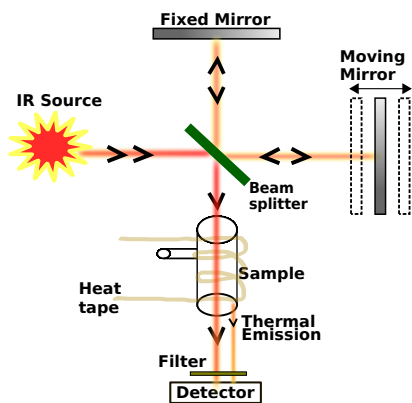


Figure 1: Schematic view of the Bruker 125HR IFS spectrometer: both the sample gas cell and the heat tape are located inside the evacuated sample compartment. The infrared emission from the gas cell does not contribute to the interferogram, and the AC-coupled detector also automatically eliminates infrared emission of the gas cell. Additionally, fused silica and Ge filters were used between sample and detector to prevent detector saturation.

sealed. After sealing the gas cell at room temperature with known number densities of CH_4 and H_2 , FTIR transmittance spectra of each tube were recorded at three different temperatures: 300, 500, 700 K. Table 1 reports the experimental conditions in detail.

Overall, 12 different spectra of CH_4 were recorded at various resolutions. Figure 2 represents an overview of spectrum #4 (i.e., $P_{\text{CH}_4}=1.1$ Torr and $P_{\text{H}_2}=100.0$ Torr), which encompasses P , Q , and R branches up to $J''=17$. In addition, each J'' consists of a cluster of transitions with various symmetry species and N quantum index¹. Figure 3 illustrates the modeled spectra for $P(7)$ transitions. The elevated temperature gas pressures, P_{CH_4} and P_{H_2} , were then calculated using the ideal gas law. Table 2 lists the resolution, number of scans, and the P_{CH_4} and P_{H_2} values for all measurements. Spectrum #1 was used to measure the unbroadened Doppler-width and intensity of each line.

The decomposition of CH_4 is an important issue for high-temperature measurements [49]. To decrease the potential for loss of CH_4 , we added 10 Torr of H_2 into the

¹ The CH_4 energy levels are labelled by different quantum numbers such as J and C (tetrahedral symmetry), and N (quantum index) defined in Brown et al. [48].

Table 1: Experimental conditions and characteristics of the spectra.

Parameter	Value
Spectral coverage	2800 – 3200 cm^{-1}
Temperature range	300 – 700 K
CH_4 pressure	0.8 – 7.0 Torr
H_2 pressure	10.0 – 933.3 Torr
Cells path length	10.0 \pm 0.2 cm
Number of averaged scans	100 – 400
Gas cell material/windows	Quartz (SiO_2)
Gas cell transmission range	2750 – 3250 cm^{-1}
Light source	SiC Globalar
Beam splitter	KBr
Detector	MCT LN2
Filter	fused silica and Ge
Spectral resolution (cm^{-1})	0.01 – 0.005
Apodization function	Box-car

first gas cell at room temperature. The main product of $\text{CH}_4 + \text{CH}_4$ bimolecular dissociation in the absence of H_2 is CH_3 , but in the presence of H_2 gas as a third-body component, CH_4 will reform. In other words, H_2 gas will decrease the amount of decomposition by increasing the back reaction. Additionally, 10 Torr of H_2 has a negligible pressure-broadening effect. The volume mixing ratios of these gases can be calculated through minimizing Gibbs free energy which is dependent on the temperature, pressure, and gas concentrations. Therefore, we used the online thermodynamical simulator² to calculate the fraction of decomposition of pure CH_4 at different temperatures and pressures. Table 3 (case 1) represents the thermodynamic mixing ratios of 0.8 Torr of pure CH_4 . Note that these calculations are done up to 900 K while the maximum laboratory temperature in this work is 700 K. Thermal decomposition of pure CH_4 is predicted to occur for temperatures 700 K and above but is suppressed by the mixture of a small amount of H_2 . Ultimately, no significant decrease of the CH_4 column density was noted even at 700 K. In this study, the line assignments and the line positions of CH_4 were adopted from HITRAN2016 [50, 51].

The CH_4 and H_2 gases were 99.99% and obtained from Matheson. The gas pressure while filling the sample

²<http://navier.engr.colostate.edu/code/code-4/index.html>

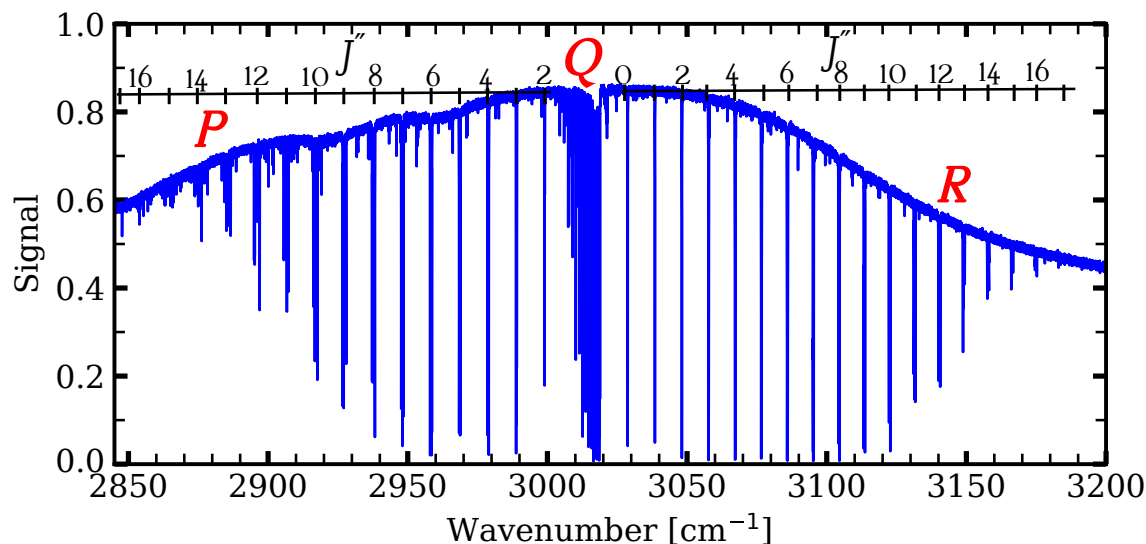


Figure 2: The measured spectrum of the CH₄ ν_3 band: $P_{\text{CH}_4}=1.1$ Torr and $P_{\text{H}_2}=100.0$ Torr. The strong lines ($J''=0-17$) belong to the ν_3 band consisting of P, Q, and R branches. Weak lines belong to $\nu_3 + \nu_4 - \nu_4$ and $\nu_2 + \nu_3 + \nu_2$ combination bands.

Table 2: Summary of the experimental conditions

#	Tube	T [K]	R^\dagger [cm ⁻¹]	Scan [‡]	P_{CH_4} [Torr]	P_{H_2} [Torr]
1	1	300	0.005	400	0.8	10.0
2	1	500	0.005	200	1.3	16.7
3	1	700	0.005	200	1.9	23.3
4	2	300	0.01	150	1.1	100.0
5	2	500	0.01	100	1.8	166.7
6	2	700	0.01	100	2.6	233.3
7	3	300	0.01	200	2.2	200.0
8	3	500	0.01	200	3.7	333.3
9	3	700	0.01	200	5.1	466.7
10	4	300	0.02	100	3.0	400.0
11	4	500	0.02	100	5.0	666.7
12	4	700	0.02	100	7.0	933.3

Tube lengths are 10.3, 9.8, 10.2, and 9.9 cm, respectively.

[†]Spectral resolution.

[‡]Number of scans averaged.

tubes was measured using two different MKS Baratron pressure gauges (maximum range 100 and 1000 Torr). For controlling the temperature, heat tapes from BriskHeat company (Type BW0) were used. A thermocouple connected to each gas cell was used in a feedback loop with the heat-tape controller to maintain a constant tempera-

Table 3: Predicted thermodynamic CH₄ volume mixing ratios[†]

T (K)	CH ₄ (%)	H ₂ (%)	C ₂ H ₂ (%)	C ₂ H ₄ (%)
Case 1: pure (100%) 0.8 Torr of CH ₄ at 300 K [‡]				
300	100	0.0	0.0	0.0
500	99.9	0.01	0.0	0.0
700	98.6	0.9	0.0	0.5
900	81.2	13.1	1.7	4.0
Case 2: 0.8 (7.4%) CH ₄ in 10.0 Torr (92.6%) H ₂ at 300 K ^{††}				
300	7.4	92.6	0.0	0.0
500	7.4	92.6	0.0	0.0
700	7.4	92.6	0.0	0.0
900	7.4	92.6	0.0	0.0

[†]These mixing ratios are calculated by minimizing the Gibbs free energy of an ideal gas mixture.

[‡]The reported pressure in each case is for 300 K. P_{H_2} and P_{CH_4} at high temperatures are calculated using ideal gas law.

^{††}In this study, 10 Torr of H₂ gas added in order to suppress the CH₄ decomposition.

ture. Omega company states typical uncertainties as 0.1% of the displayed reading for their digital readers. The uncertainty for type K probes is estimated to be 0.75% (2.2 K at 300 K). Therefore, the overall uncertainty is due to the probe, not the reader, and T is good to within ± 2 K at the location of the junction. There is a possibility of temperature nonuniformity in our gas cell. We expect this effect to be small given the high heating-element coverage of the cell excluding the transmitting windows but including its support structure, the small size of the cell,

and its vacuum environment. The uncertainty in the measurement of P_{H_2} and P_{CH_4} is less than 0.5%, and is also negligible.

3. Data Analysis

Our main goal is to extract pressure-induced broadening coefficients by modeling all lines with Voigt line profiles. Lorentzian and temperature-dependence coefficients for each rovibrational line are determined from linewidths extracted from spectra #1–12 using a least-squares fitting method. The signal-to-noise ratio (S/N) is insufficiently high to justify modeling the spectra with non-Voigt profiles.

The negligibly pressure-broadened sample tube # 1 was analyzed first to determine the correct CH₄ line assignments, wavenumber calibration, and the presence of other CH₄ bands and other contaminant species. Line strengths were determined separately at each measured temperature. The highly-blended pressure-broadened spectra were analyzed with line strengths fixed to their unbroadened values and line widths and positions freely modified.

3.1. Continuum / baseline fitting

All CH₄ spectra were converted from their interferograms with a Boxcar apodization using the OPUS software³. The effect of instrumental broadening was modeled using a custom fitting code as a sinc function [52]. The background continuum is also modeled using cubic splines optimised during the least-squares fitting procedure [53]. Additionally, interference between the two cell windows that affects the recorded spectra by introducing sinusoidal behavior into the spectral continuum. We modeled this interference effect by employing two sine functions scaling the modeled spectrum.

3.2. Line position corrections

Line assignments are determined from the recent version of HITRAN [50, 51]. All corresponding line positions from HITRAN were input into the fitting code, and a global fit was made to calculate a single global shift induced by any slight miscalibration of the spectrometer. Afterward, the calculated shift was applied to our

low pressure spectra (i.e., spectra #1–3 in Table 2). Later, the corrected/shifted line positions from the low pressure spectra were used to fit high pressure spectra (i.e., spectra #4–12 in Table 2), where pressure-induced lineshifts were also evident.

3.3. Line profiles

At very low pressure, the effect of collisions on molecular spectra is negligible. However, molecular velocities are distributed according to the Maxwell–Boltzmann statistics resulting in Doppler broadening (see chapter 1 at [54]). The Doppler half-width at half-maximum (HWHM) linewidth (Γ_{D}) were individually modeled using Gaussian line profile f_{G} :

$$f_{\text{G}}(\nu - \nu_{ij}, \Gamma_{\text{D}}) = \sqrt{\frac{\ln(2)}{\pi \Gamma_{\text{D}}^2}} \exp\left(-\frac{\ln(2)(\nu - \nu_{ij})^2}{\Gamma_{\text{D}}^2}\right) \quad (1)$$

$$\Gamma_{\text{D}}(T) = \frac{\nu_{ij}}{c} \sqrt{\frac{2 \ln(2) N_{\text{A}} k_{\text{B}} T}{M}} \quad (2)$$

where M is the molar mass of the absorber molecule in grams, N_{A} is the Avogadro constant, k_{B} is the Boltzmann constant, and ν_{ij} is the line position or the energy gap between quantum levels i and j in any arbitrary energy unit (e.g., cm^{-1}). Γ_{D} values for our various measurements are in the range 0.004 – 0.007 cm^{-1} given the dependence of Γ_{D} on the temperature and wavenumber. The natural radiative linewidth of the CH₄ ν_3 band is $\sim 10^{-9} \text{ cm}^{-1}$ (i.e., in the range of 10–100 Hz) [55], which is fully negligible when fitting the spectra.

Since the intensity of each line is distributed as a result of pressure-broadening, we increased the column density of CH₄ when a high H₂ pressure is present in order to obtain optimal S/N ratios without saturating any lines. As a result of this change, the modeled CH₄ optical depth of high-pressure spectra (i.e., spectrum # 4–12) were scaled up uniformly.

The Lorentzian HWHM linewidth Γ_{L} and lineshift Δ_{L} were fitted individually for each line using the Lorentzian line profile f_{L} :

$$f_{\text{L}}(\nu; \nu_{ij}, \Gamma_{\text{L}}, \Delta_{\text{L}}) = \frac{1}{\pi} \frac{\Gamma_{\text{L}}(p, T)}{[\Gamma_{\text{L}}(p, T)]^2 + [\nu - (\nu_{ij} + \Delta_{\text{L}})]^2} \quad (3)$$

³www.bruker.com

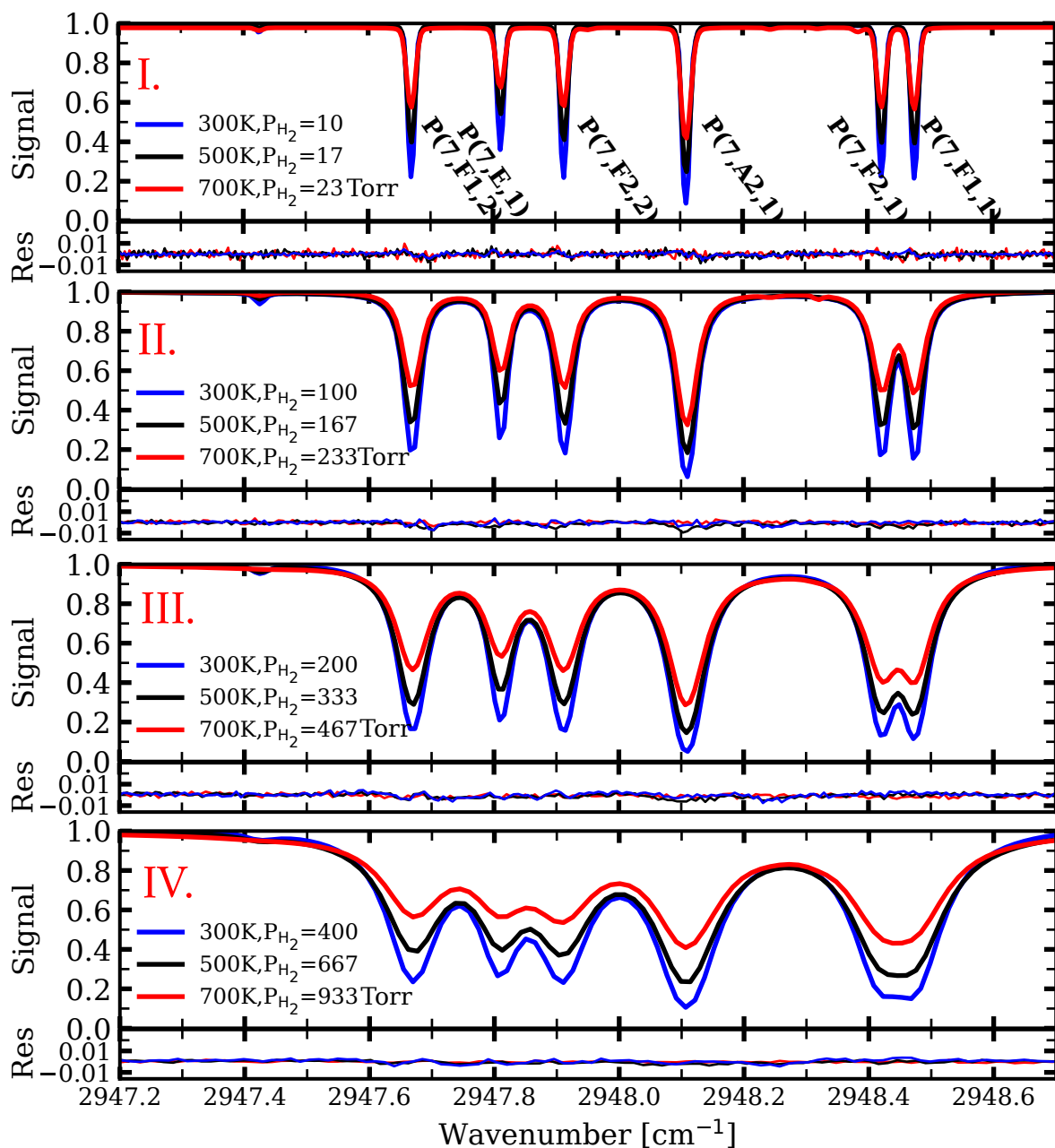


Figure 3: Examples of recorded spectra showing the $P(7)$ cluster of the ν_3 band of CH_4 in a H_2 bath gas: In this study, four quartz cells (I–IV) with different amounts of P_{CH_4} and P_{H_2} (i.e., P_{CH_4} (Torr) : P_{H_2} (Torr) = 0.8:10, 1.1:100, 2.2:200, 3.0:400) were used to record the FTIR transmittance spectra of CH_4 in H_2 at 300 K (blue), 500 K (black), and 700 K (red). Transitions with E symmetry are weaker than A_1/A_2 and F_1/F_2 symmetries for similar quantum number J . The measured resolution for these 12 spectra varies from 0.005 cm^{-1} for the lowest pressure (panel I) to 0.02 cm^{-1} for the highest pressure (panel IV, 700 K). A least-squares fitting procedure with Voigt line profiles was employed to model the spectra. The residual (Res) subpanels represent difference between modeled and recorded spectra. In addition, we also find lines from other bands such as $2\nu_2$ and $\nu_2 + \nu_4$ bands; however, their S/N is not strong enough for pressure-broadening analysis.

$$\Gamma_L = \left(\frac{T}{T_0}\right)^{-n_\gamma} \gamma_L P_{\text{H}_2} \quad (4)$$

$$\Delta_L = \left(\frac{T}{T_0}\right)^{-n_\delta} \delta_L P_{\text{H}_2} \quad (5)$$

in which γ_L ($\text{cm}^{-1}/\text{atm}$) and n_γ are the Lorentzian linewidth coefficient and its temperature-dependence coefficient, respectively. δ_L ($\text{cm}^{-1}/\text{atm}$) and n_δ are the Lorentzian lineshift coefficient and its temperature-dependence coefficient, respectively. T_0 is a reference temperature, and it is set equal to 300 K. Note, all these coefficients are dependent on the total rotational quantum number of J , tetrahedral (T_d) symmetry species, and the broadeners. The code computes the Voigt profile as the Faddeeva function.⁴

The Lorentzian coefficients Γ_L , extracted from the recorded spectra result from the effect of P_{H_2} collisional-induced broadening. The pressure-broadening from CH_4 self broadening is negligible since $P_{\text{CH}_4} \leq 1.1\% \times P_{\text{H}_2}$. Regarding Dicke narrowing, this effect becomes important at intermediate pressures or the Doppler–Lorentzian transition region because Doppler broadening at low pressures and Lorentzian broadening at high pressures mask the narrowing. For example, Pine [35] found the largest discrepancy between Voigt and Rautian at 50 Torr H_2 , and a corresponding 5% difference in the derived γ_L for the two cases. This difference will be reduced by about half at 100 Torr (the lowest pressure we use). Then our Lorentzian linewidths fitted at 100 Torr may be underestimated by up to 3% (in comparison with random fitting uncertainties of at 4% or more).

Other formulations for the temperature-dependence of Eq. 5 have been adopted elsewhere [47]. We use the most conventional single-parameter temperature dependence formula above given the limited temperature sampling of our data.

4. Results and Discussion

4.1. Pressure broadening coefficients: γ_L and n_γ

After fitting all 12 spectra from 300 to 700 K, the Lorentzian HWHM (i.e., Γ_L in Eq. 4) is extracted for each

tetrahedral rovibrational transition⁵. Then, the γ_L and n_γ coefficients are computed in three different ways: 1) for all lines individually including its own J , symmetry and N numbers, 2) averaged over lines with the same J'' but different symmetry and N index (i.e., the multiplicity index), and 3) all lines with the same J'' and symmetry but different N index were fitted. As a sample fitting, Fig. 4 illustrates Γ_L versus $(T/300 \text{ K})^{-n_\gamma} P_{\text{H}_2}$ for $J''=7$ and different symmetry species (n_γ is computed below). Figure 4 shows the fitted slope (i.e., γ_L) of transitions with A_1/A_2 and F_1/F_2 is higher than for the E symmetry lines.

Figure 5(I–III) illustrates the trend of γ_L and n_γ with J'' . Figure 5(I) represents γ_L and n_γ fitted to all lines individually. At each J'' value, there is the scatter of both γ_L and n_γ coefficients which arise from the difference between T_d symmetries, N indexes, and random fitting errors. In the first analysis step, individual lines with the same J , symmetry, N from all spectra were fitted to extract the γ_L and n_γ coefficients data. From this we determine the Lorentzian linewidth of each individual line as a result of H_2 collisional impact. Figures 4 and 5(I) as well as the supplementary Table (S1) represent these results. The error bars shown in these figures and the table uncertainties are due to the fitting uncertainties, noise, and the low signal-to-noise of some lines. These line-by-line coefficients are the main outcome of this study and they can be utilized in generating absorption cross-section (or opacity) data the standard HITRAN code⁶ or the NASA Ames Freedman’s code [19, 57].

In contrast, if we average the coefficients for all lines with the same J'' value, then γ_L and n_γ coefficients fall in the range of 0.07–0.03 and 0.65–0.25, respectively (see Fig. 5(II) and Table 4). In Table 4, the scatter of these coefficients are mostly due to the scattering of lines with the same J'' but different symmetries and N dependencies, as well as, the uncertainty in fitting the Lorentzian linewidths from the recorded spectra. Another motivation for this step is to provide data for opacity codes which input only J -dependent pressure-broadening val-

⁴http://ab-initio.mit.edu/wiki/index.php/Faddeeva_Package

⁵ Each tetrahedral transition is labelled by total rotational quantum number J , symmetry species C , and quantum index N [48].

⁶i.e. HITRAN Application Programming Interface (HAPI) [56], <https://github.com/hitranonline/hapi>

ues such as the current version of EXOCROSS code⁷[58]. Figure 5(II) shows that there is a clear dependency of the Lorentzian coefficient and its temperature-dependence with (γ_L and n_γ) on J . This data are also presented in Table 4, and the range of scatter for each one is shown as a range of $\gamma_L^{\min}-\gamma_L^{\max}$ and $n_\gamma^{\min}-n_\gamma^{\max}$. According to the Anderson collisional theory [40], the n_γ coefficient is expected to be 0.5; however, our analysis shows that n_γ coefficients deviate from this value by up to 30%. We also find that γ_L and n_γ decrease by 25% and 80%, respectively, between $J''=2$ and 17 in agreement with the trend calculated by Neshyba et al. [45] and Gabard [44].

Next, we grouped the lines with similar symmetries, and extracted the Lorentzian coefficients from each group. Figure 5(III) shows the symmetry-dependence of γ_L and n_γ . The bars shown in this figure are due to the uncertainty in fitting this data (similar to Fig. 5(III)) and also the scatter imposed by different values of the N quantum index. It should be noted that only some symmetry- J combinations have multiple N values. Therefore, two kinds of uncertainties are shown in Table 7: statistical fitting uncertainties for singular- N values, and the range of scatter for values averaged over multiple N transitions. In general, within each J manifold, E -lines are the weakest and also have the narrowest Lorentzian linewidth Γ_L . In contrast, lines with A_1/A_2 and F_1/F_2 symmetries are generally the strongest, and have the broadest linewidth.

Following the complex Robert-Bonamy theory[59], Neshyba et al. [45] calculated the impact of electrostatic and atom-atom intermolecular potential on the line broadening and line shift of the CH₄@[N₂] system. They found that the atom-atom potential component is the main reason for the line broadening with a corresponding decrease with increasing total angular momentum, J . In addition, the broadening effect is symmetry dependent and it was shown [44, 47, 60] the total collisional cross-section for E symmetry is lower than for A_1/A_2 and F_1/F_2 at low J , which results in smaller perturbation and collisional-broadening for the E -symmetry species, as we observed.)

4.2. Lorentzian temperature-dependence coefficient: n_γ

According to early Anderson collisional theory [40, 61] a broadened line has a Lorentzian profile (Eq. 3), and the

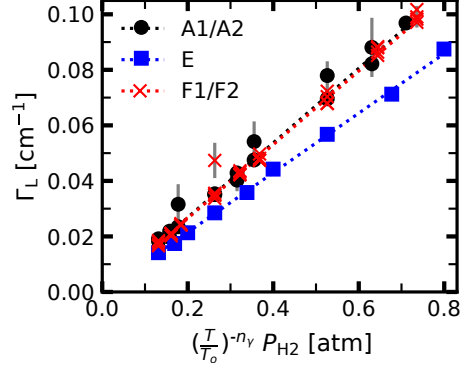


Figure 4: Lorentzian linewidth Γ_L versus $(T/T_0)^{-n_\gamma} P_{H_2}$ for all transitions with $J''=7$: This plot shows that the Lorentzian coefficients are strongly dependent to the T_d symmetry, and in most cases, γ_L for E symmetry is smaller than A_1/A_2 or F_1/F_2 symmetries. Each point has its own error bar, which represents the uncertainty in fitting the Γ_L linewidths. In addition, there are multiple lines with different N -index for the A_1/A_2 and F_1/F_2 symmetries. Where error bars are not visible, the uncertainties are smaller than the symbol size.

broadening linewidth is proportional to $T^{-0.5}$ following Eqs. 6 and 7:

$$\Gamma_L = \frac{n\bar{v}_{th}\sigma_r}{2\pi} \quad (6)$$

where n is the broadener column density (i.e., $n=n_{H_2}=P_{H_2}/k_bT$), \bar{v}_{th} is the mean thermal velocity from Maxwell-Boltzmann distribution (i.e., $\bar{v}_{th} = \sqrt{8k_bT/\pi m}$ where m is the H₂ mass), and σ_r is the real component of the collisional cross-section (see discussion in [62]).

$$\Gamma_L = \sqrt{\frac{2}{k_B m \pi^3}} P_{H_2} T^{-0.5} \sigma_r \quad (7)$$

Following Eqs. 6 & 7, the temperature-dependence coefficient, n_γ is 0.5. Note, there are different assumptions at play in Eq. 7 including the hard-sphere approximation, ideal gas law, and also a single thermal velocity \bar{v}_{th} for all broadeners. Therefore, this $n_\gamma=0.5$ value should be considered as a gas kinetic value, and a more sophisticated picture is reviewed by Gamache and Vispoel [63]. Our results show that n_γ strongly depends on J , and it is in the range of $\sim 0.65-0.2$ (see Fig. 5(II)). No significant dependence of n_γ on the tetrahedral symmetry species is found.

Table 5 lists most previous temperature-dependence measurements of CH₄ in different broadeners. In addition, the measurements are for different fundamental and

⁷<https://github.com/Trovemaster/exocross>

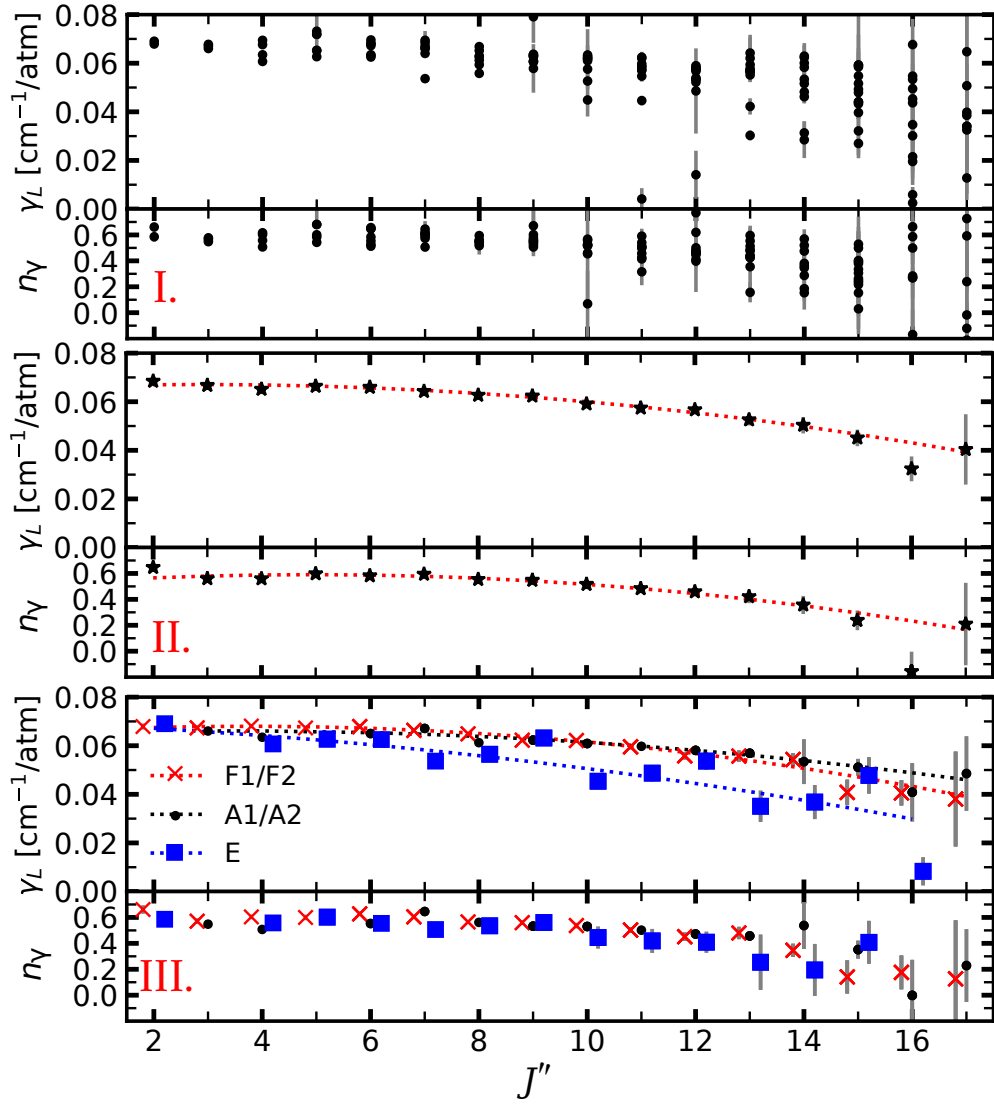


Figure 5: Dependence of the Lorentzian coefficients γ_L and n_γ on quantum number J'' . Panel I: All lines were fitted individually. The uncertainties are $1\text{-}\sigma$ error in each individual line but the scatter arises primarily from the symmetry and N -index. Panel II: Average of all lines over symmetry and N index. However this approach ignores the dependence of symmetry and N dependency, and therefore, it disregards these important physical effects. Panel III: Average of all lines within a symmetry species. γ_L and n_γ are reported in Tables 4, 7, and in the Table S1 (supplementary file). Note that a few points are out of the fitted trend (dotted line), and therefore, the fitted coefficients are reported in these tables. In addition, weak lines with low S/N ratio and high-uncertainty are removed from the list in Table S1 (supplementary file). Where error bars are not visible, the uncertainty from fittings for the data is smaller than the symbol size itself.

combination vibrational modes providing insight into the vibrational dependency of n_γ . The n_γ of CH₄@[N₂] and CH₄@[Air] falls in the range of $\sim 0.55\text{--}1.0$ and $\sim 0.4\text{--}0.9$,

respectively, which are roughly 30% larger than our results for CH₄@[H₂]. In comparison, CH₄@[He] is about half that of CH₄@[H₂]. Table 5 also illustrates the slight

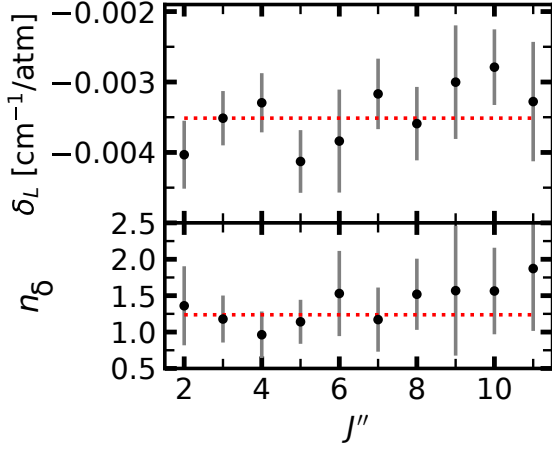


Figure 6: The dependency of pressure shift on quantum number J'' . The plotted error-bars are an indistinguishable combination of fitting uncertainties and differences between symmetry and N quantum index.

vibrational-dependency of n_γ for various broadeners.

4.3. Lorentzian line-shift coefficients: δ_L and n_δ

The S/N ratio in the current study is insufficiently high to extract pressure shifts for all lines. Hence, a pressure-shift coefficient is calculated only for lines with $J''=2-11$, and falls in the range of -0.004 to -0.002 $\text{cm}^{-1}/\text{atm}$. We discern no significant dependence of the Lorentzian pressure-shift coefficients on the J values (Fig. 6), and the mean value of δ_L and n_δ are -0.0035 $\text{cm}^{-1}/\text{atm}$ and 1.24, respectively. The reported uncertainties for Lorentzian pressure-shift coefficients (δ_L and n_δ) are due to the scatter of the symmetry- and N -dependency. Note that our n_δ is larger than n_γ , and this difference has been reported for water self-broadening as well [70].

The form of Eq. 5 is based on Eq. 4, which is derived from the ideal gas law and hard-sphere approximation. Some studies of other systems such as Frost [41] and Baldacchini et al. [71] have shown temperature-dependence has more complex form than our selected formula in Eq. 5. Additionally, Smith et al. [47] found both positive and negative δ_L and n_δ values for the CH_4 ν_4 band. However, we exclusively observed negative δ_L and positive n_δ values.

Table 4: J -dependent Lorentzian coefficients averaged over ν_3 P branch line cluster of CH_4 .

J'	J''	γ_L	$\gamma_L^{\min}-\gamma_L^{\max}$ *	n_γ	$n_\gamma^{\min}-n_\gamma^{\max}$ *	δ_L^\dagger	n_δ
1	2	0.069	0.068–0.069	0.65	0.59–0.66		
2	3	0.067	0.066–0.068	0.56	0.55–0.57	–0.0040(5)	1.4(5)
3	4	0.065	0.061–0.068	0.56	0.51–0.60	–0.0035(4)	1.2(3)
4	5	0.066	0.063–0.067	0.60	0.54–0.68	–0.0032(4)	1.0(3)
5	6	0.066	0.063–0.068	0.58	0.55–0.63	–0.0041(4)	1.1(3)
6	7	0.064	0.054–0.067	0.59	0.51–0.65	–0.0038(7)	1.5(6)
7	8	0.063	0.057–0.061	0.55	0.54–0.57	–0.0031(5)	1.2(4)
8	9	0.063	0.062–0.063	0.55	0.53–0.56	–0.0035(5)	1.5(5)
9	10	0.059	0.045–0.062	0.52	0.44–0.54	–0.0030(8)	1.6(9)
10	11	0.058	0.049–0.060	0.48	0.42–0.52	–0.0027(5)	1.6(6)
11	12	0.057	0.054–0.058	0.46	0.41–0.47	–0.0032(8)	1.9(9)
12	13	0.053	0.035–0.057	0.42	0.25–0.48		
13	14	0.051	0.037–0.054	0.36	0.20–0.54		
14	15	0.046	0.041–0.051	0.24	0.14–0.41		
15	16	0.043 [‡]		0.24 [‡]			
16	17	0.041	0.038–0.049	0.20	0.14–0.65		

Note:

* $\gamma_L^{\min}-\gamma_L^{\max}$ and $n_\gamma^{\min}-n_\gamma^{\max}$ represent the range of coefficients before averaging over symmetry and N . Only the lines with high S/N ratios are considered for extracting the Lorentzian pressure-shift coefficients (δ_L and n_δ).

[†]The scattering in the pressure-shift coefficients arises from their dependencies into the symmetry and N .

[‡]The extracted values of γ_L and n_γ for $J''=16$ are 0.0324(51) and $-0.2(1)$, which are out of the trend. Therefore, these values are replaced with the expected values from the polynomial equation 8 due to the weakness of the lines.

4.4. Global equations for Lorentzian coefficients

In order to provide Lorentzian broadening coefficients (γ_L and n_γ) appropriate for high-temperature H_2 -dominated exoatmospheres (i.e., super-Earth or warm-Neptunes with 400–900 K temperature), the dependency of these coefficients with J'' is presented by fitting the experimental results to a second-order polynomial J'' -dependence (e.g., Eq. 8 see the red-dashed line in Fig. 5(II)). Additionally, due to the significant dependence of γ_L on the symmetry species, the fitting coefficients are extracted from them separately (i.e., Eq. 9 dashed lines in Fig. 5(III)) conforming to:

$$X(J'') = m_1 + m_2 J'' + m_3 J''^2 \quad (8)$$

$$X(J'', \text{sym}) = m_1 + m_2 J'' + m_3 J''^2 \quad (9)$$

where m_1 , m_2 , and m_3 are the fitted constants, X is the Lorentzian coefficient i.e., γ_L , n_γ , and “sym” can be A_1/A_2 , F_1/F_2 , or E symmetry species. All the polynomial fitted constants are presented in Table 6.

Table 6: Fitted constants for global equations[†]

Case	m_1	m_2	m_3
$\gamma_L (J'')$	0.066	0.0008	-0.00014
$n_\gamma (J'')$	0.520	0.0290	-0.00290
$\gamma_L (J'', F_1/F_2)$	0.0657	0.0012	-0.00017
$\gamma_L (J'', A_1/A_2)$	0.0650	0.0007	-0.00011
$\gamma_L (J'', E)$	0.0690	-0.0010	-0.00010

[†]Eqs. 8 and 9 are used to fit the γ_L and n_γ results.

Note: γ_L and n_γ coefficients are reported in Table S1 for all ν_3 P -branch lines. The polynomial equations Eqs. 8 and 9 should be used to determine these coefficients for transitions in the range of $J''=0-18$.

4.5. Comparison with existing data

Since CH₄ is an important molecule in the atmosphere of the Earth, other planets, and brown dwarfs, many experiments have been carried out for broadeners in the atmosphere of Earth (i.e., N₂ and O₂), Jupiter (i.e., H₂ and He), and other broadeners such as Ar- and self-broadening. In the following, we will discuss the comparison of our results with the most relevant literature data.

Figure 7 represents the comparison of our results with the literature data [35, 65, 66, 72, 73] for the CH₄@[H₂] ν_3 band. Note that most of the previous studies have been for the Q branch [35, 72] and employed Rautian line profiles; while there are a few measurements on the P branch [65, 73], none employ H₂ as a broadener. Figure 7 (I,II) shows the comparison of all lines with their J -, symmetry- and N -dependencies. In Fig. 7 (II), the Pine [72] results are slightly lower than ours which might be due to the selection of different line profiles and branches. In Fig. 7, a comparison of lines within different symmetry classes is shown.

Figure 8 illustrates the comparison between our temperature-dependence coefficients n_γ (i.e., CH₄@[H₂] for ν_3 P branch) with both CH₄@[N₂] and CH₄@[Air] for ν_4 band. Note, there are a two differences between these measurements: 1) our broadener H₂ is different from the previous works, 2) there might be some vibrational-dependency of n_γ . In general our n_γ coefficients (@[H₂]) is smaller than both @[Air]-broadening and @[N₂]-broadening 5.

Figure 9 represents the effect of various broadeners (i.e., self or CH₄, N₂, and He) on γ_L for different T_d symmetry species [35, 43, 65, 66, 72, 73]. In general $\gamma_L(\text{Self}) > \gamma_L(\text{H}_2) \geq \gamma_L(\text{N}_2) > \gamma_L(\text{He})$. In earlier work [42], electrostatic forces (dipole, quadrupoles, and higher-order

multipoles) were theorised to cause the differing broadening effects of various broadeners (or perturbers) on CH₄. However, the quadrupole moments of O₂ and N₂ could not explain their similar broadening of CH₄ (e.g., [43]), given that their quadrupole moments differ by a factor of 3. Later, Neshyba et al. [45] showed that in fact atom-atom interactions supplant electrostatic interactions is a minor reason, and atom-atom interaction is the major source of broadening using Robert-Bonamy theory [59] (see the theory section in Ref. [44]).

Figure 10 compares our Lorentzian pressure-shift results $\delta_L(\text{CH}_4\text{@[H}_2\text{]})$, P branch, see Table 4) with literature values for different broadeners and branches. The reported δ_L are averaged over of J'' , and they are in the range of the Pine [35] ν_3 Q -branch data. In addition, this figure shows that the collisional effect of N₂ and Ar species on pressure shift is larger than H₂. The largest δ_L , however, would be due to the CH₄ self-broadening interactions, and it is $\sim 2\times$ higher than our results ($\delta_L(\text{CH}_4\text{@[H}_2\text{]})$).

5. Summary & Conclusion

High-temperature Lorentzian broadening and shift coefficients of CH₄@[H₂] for more than 100 individual rovibrational transitions in the ν_3 P branch are obtained using high resolution (0.01–0.005 cm⁻¹) FTIR spectroscopy. We find that γ_L falls in the range 0.03–0.07 cm⁻¹/atm, and is strongly dependent on molecular rotation and symmetry dependent. The temperature-dependence broadening coefficient, n_γ falls in the range 0.20–0.65. The averaged shift pressure and its temperature-dependence coefficient, δ_L and n_δ are -0.0035 cm⁻¹/atm and 1.24, respectively, and these are constant with J as far as our data can determine.

All these coefficients were fitted to simple polynomial equations in terms of J'' and neglecting symmetry and N quantum index for the benefit of the astrophysical/exoplanetary community. Table S1 lists the γ_L and n_γ for all individual lines, showing the change in these coefficients with J , symmetry, and N numbers, and is recommended to use these data where these details are important. The detection of CH₄ spectral features in hot-Jupiters to super-Earths needs these pressure-broadening data because of their high-temperature and H₂-dominant atmospheres.

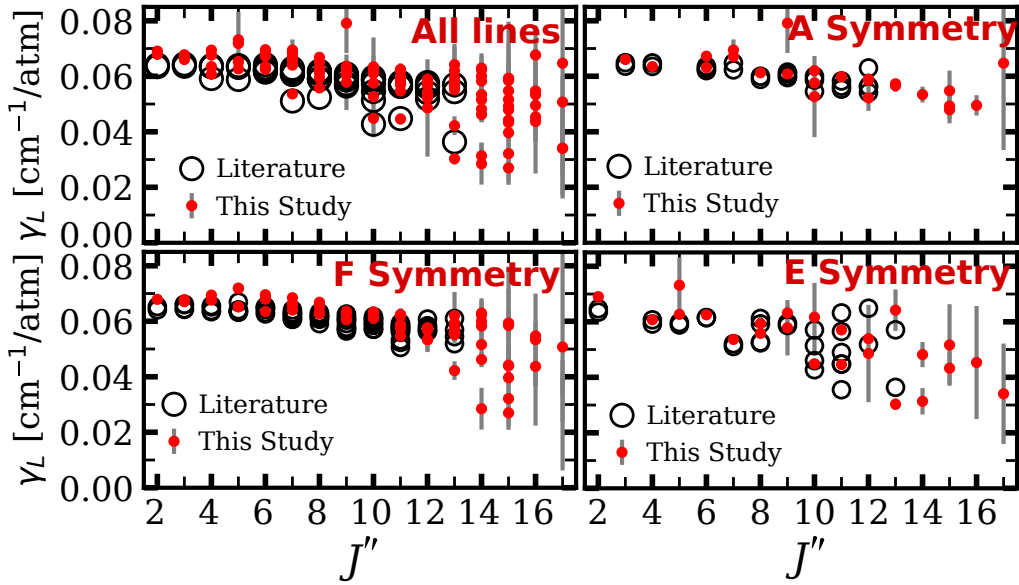


Figure 7: Comparison of our γ_L results with literature pressure-broadening coefficients of ν_3 Q -branch $\text{CH}_4@[\text{H}_2]$ [35, 72], and ν_3 P -branch $\text{CH}_4@[\text{H}_2]$ [73]. Where error bars are not visible, the uncertainties for our γ_L are smaller than the symbol size itself.

These pressure-broadening and pressure-shift coefficients can be directly incorporated into current databases, such as HITRAN/HITEMP or EXOMOL.

6. Acknowledgment

We kindly thank Glenn Stark, David Wright, Adam Schneider, and the Arizona State University exoplanet group for many useful discussions. E.G.N. especially thanks Mike Line for invaluable numerous invaluable discussions during this work as well as Richard Freedman and Mark Marley invaluable discussions regarding the intricacies of opacity data. E.G.N. acknowledges funding from the GRSP research grant from the Arizona State University Graduate office program award XH51027. A.N.H.'s research was supported by an appointment to the NASA Postdoctoral Program at Arizona State University and the NASA Astrobiology Institute, administered by Universities Space Research Association under contract with NASA. This research used resources of the Advanced Light Source, which is a DOE Office of Science User Facility under contract no. DE-AC02-05CH11231.

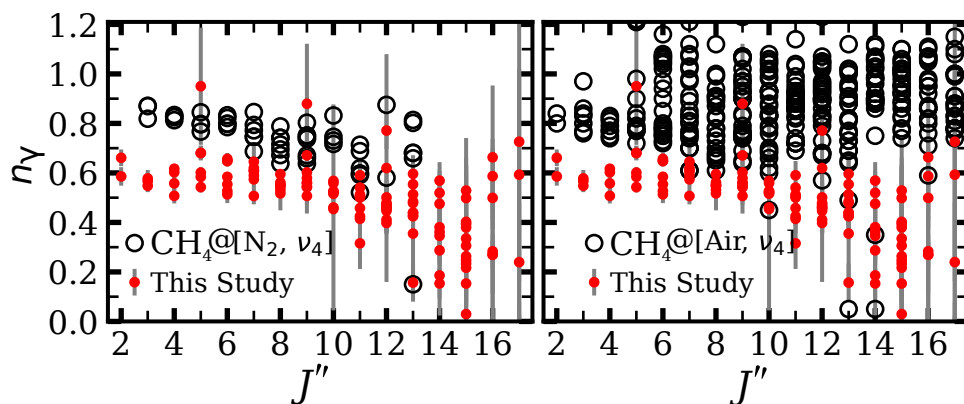


Figure 8: Comparison of our temperature-dependence coefficients (i.e., ν_3 P -branch $\text{CH}_4@[\text{H}_2]$) at temperature range 300–700 K with ν_4 Q -branch $\text{CH}_4@[\text{N}_2]$ Smith et al. [47] and ν_4 P - and R -branch $\text{CH}_4@[\text{Air}]$ Smith et al. [74] at temperature range of 210–314 K.

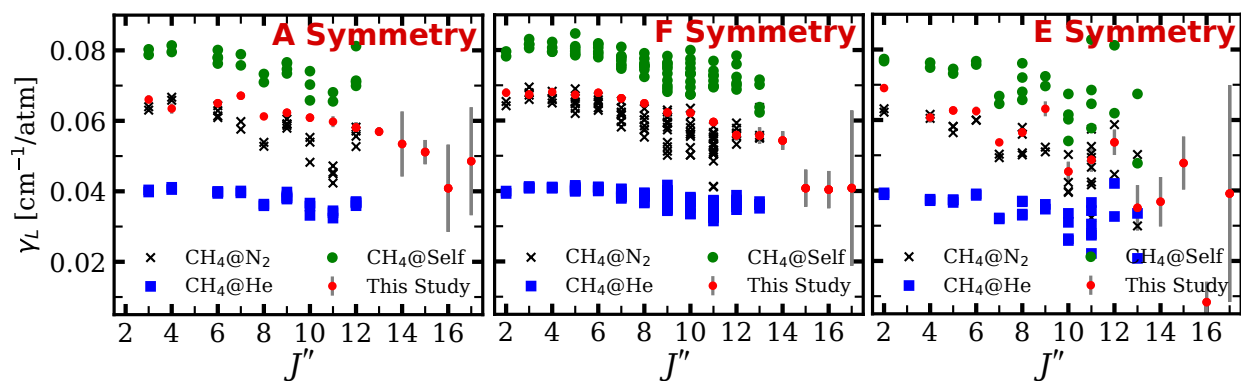


Figure 9: Comparison of our γ_L results with the literature data including ν_3 Q -branch $\text{CH}_4@[\text{He}, \text{N}_2, \text{and Self}]$ [35]. Note that our results are averaged over N , however, the scatter of the literature data arises from the N quantum index. Where error bars are not visible, the uncertainties are smaller than the symbol size.

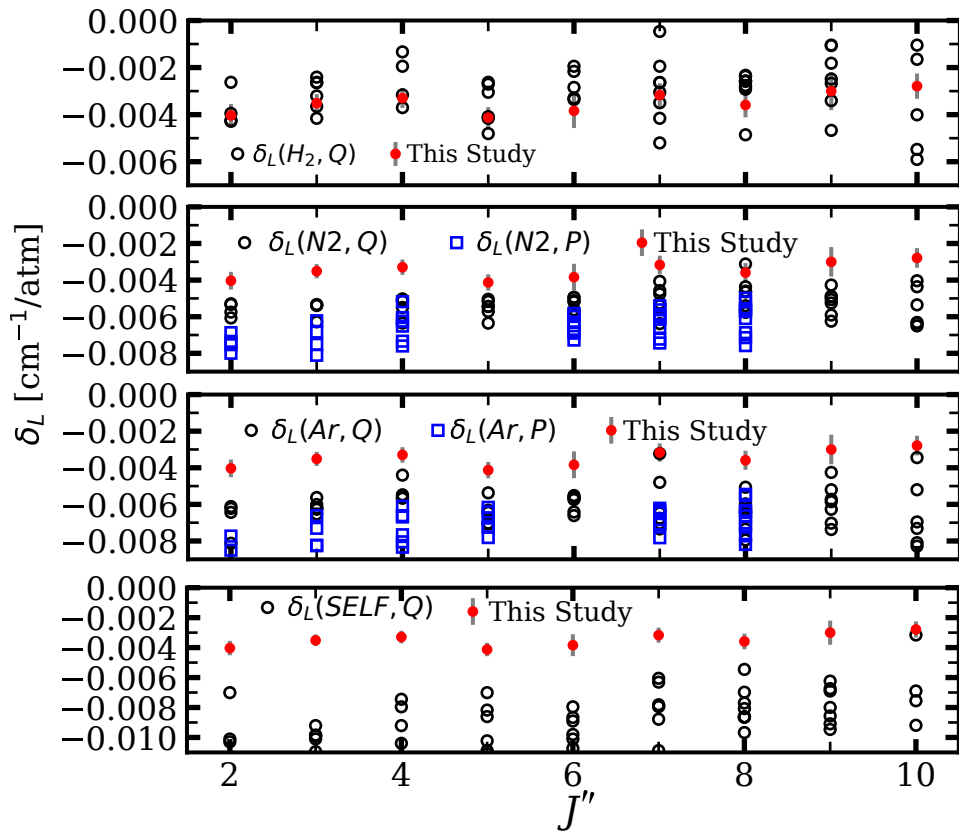


Figure 10: The comparison of pressure-shift coefficient δ_L for different broadeners (i.e., H₂, N₂, Ar, and self-broadening), and different branches Q and P [35, 72, 75].

Table 5: Overview of previous measured temperature-dependence coefficients, n_γ , of CH₄ in various broadeners

Broadener	T[K]	Band	Lines	n_γ [†]	Ref.	
H₂	300 – 700	ν_3	116	0.2 – 0.65	PS [‡]	
	77 – 295	$6\nu_1, 5\nu_3$	2	0.45, 0.53	[64]	
	130 – 295	ν_4	6	0.46 – 0.51	[65, 66]	
	161 – 295	ν_4	6	0.35 – 0.52	[67]	
Air	200 – 300	ν_3	3	0.62 – 1.0	[46]	
	211 – 314	ν_4	148	0.50 – 0.80	[47]	
	212 – 297	$\nu_1 + \nu_4$	130	0.50 – 0.85	[68]	
	212 – 297	$\nu_3 + \nu_4$	406	0.50 – 0.90	[68]	
	212 – 297	$\nu_2 + \nu_3$	71	0.40 – 0.85	[68]	
	N ₂	215 – 297	ν_3	3	0.94 – 0.97	[43]
215 – 297		$\nu_2 + \nu_4$	2	0.86, 0.92	[43]	
77 – 295		$6\nu_1, 5\nu_3$	2	0.77, 0.97	[64]	
130 – 295		ν_4	6	0.75 – 0.83	[65, 66]	
161 – 295		ν_4	6	0.71 – 0.82	[67]	
211 – 314		ν_4	148	0.55 – 0.85	[47]	
90 – 296		ν_3	4	0.84 – 0.86	[69]	
Self		77 – 295	$6\nu_1, 5\nu_3$	2	0.84, 0.93	[64]
He		77 – 295	$6\nu_1, 5\nu_3$	2	0.37, 0.67	[64]
		130 – 295	ν_4	6	0.28 – 0.38	[65, 66]
	161 – 295	ν_4	6	0.26 – 0.38	[67]	
Ar	130 – 295	ν_4	2	0.80 – 0.83	[65, 66]	
	161 – 295	ν_4	6	0.72	[67]	
				0.82		

[†] n_γ coefficients are reported within a range due to their dependency on J and vibrational quantum numbers. In this table, the reported n_γ in some cases are extracted from a few transitions.

[‡] Present Study

Table 7: Broadening coefficients* averaged over N .

J'	J''	Sym	γ_L [cm ⁻¹ /atm]	$\gamma_L^{min} - \gamma_L^{max}$	n_γ	$n_\gamma^{min} - n_\gamma^{max}$
1	2	E	0.069(1)		0.59(4)	
1	2	F	0.068(1)		0.66(3)	
2	3	A	0.066(1)		0.55(3)	
2	3	F	0.067(1)		0.57(2)	
3	4	A	0.064(2)		0.51(3)	
3	4	E	0.061(2)		0.56(4)	
3	4	F	0.068	0.068–0.069	0.60	0.60–0.62
4	5	E	0.063	0.063–0.073	0.60	0.60–0.95
4	5	F	0.067	0.065–0.072	0.60	0.54–0.68
5	6	A	0.065	0.063–0.067	0.55	0.53–0.58
5	6	E	0.063(1)		0.55(3)	
5	6	F	0.068	0.063–0.070	0.63	0.51–0.66
6	7	A	0.067	0.067–0.069	0.65	0.59–0.65
6	7	E	0.054(1)		0.51(2)	
6	7	F	0.066	0.064–0.068	0.60	0.57–0.62
7	8	A	0.061(1)		0.56(2)	
7	8	E	0.057	0.056–0.059	0.54	0.52–0.53
7	8	F	0.065	0.063–0.067	0.57	0.55–0.60
8	9	A	0.062	0.061–0.079	0.53	0.52–0.88
8	9	E	0.063	0.058–0.063	0.56	0.56–0.67
8	9	F	0.062	0.061–0.064	0.56	0.51–0.60
9	10	A	0.061	0.053–0.062	0.53	0.46–0.57
9	10	E	0.045	0.045–0.062	0.44	0.07–0.45
9	10	F	0.062	0.061–0.063	0.54	0.52–0.56
10	11	A	0.060(2)		0.50(3)	
10	11	E	0.049	0.045–0.057	0.42	0.41–0.43
10	11	F	0.060	0.055–0.059	0.50	0.32–0.59
11	12	A	0.058	0.052–0.059	0.47	0.46–0.50
11	12	E	0.054	0.049–0.054	0.41	0.40–0.62
11	12	F	0.056	0.055–0.058	0.45	0.41–0.77
12	13	A	0.057(1)		0.46(3)	
12	13	E	0.035	0.030–0.064	0.25	0.16–0.48
12	13	F	0.056	0.055–0.062	0.48	0.36–0.60
13	14	A	0.053(9)		0.54(18)	
13	14	E	0.037	0.031–0.048	0.19	0.19–0.29
13	14	F	0.054	0.052–0.063	0.35	0.15–0.57
14	15	A	0.051	0.049–0.055	0.35	0.22–0.50
14	15	E	0.048	0.043–0.052	0.41	0.31–0.40
14	15	F	0.041	0.027–0.059	0.14	0.15–0.53
15	16	A	0.048 [†]	0.041–0.068	0.24 [†]	0.24–0.59
15	16	E	0.027 [‡]		0.24 [‡]	
15	16	F	0.041	0.041–0.053	0.19	0.24–0.66
16	17	A	0.049	0.045–0.065	0.24	0.18–0.59
16	17	E	0.039	0.023–0.034	0.65	0.18–0.73
16	17	F	0.038	0.037–0.051	0.14	0.18–0.24

Note:

* The uncertainties in parentheses (in units of the least-significant digit) are derived from the estimated uncertainty of fitted linewidths. These are not well defined where lines of differing quantum index, N , have been averaged and instead the range of parameters for individual lines is given as $\gamma_L^{min} - \gamma_L^{max}$ and $n_\gamma^{min} - n_\gamma^{max}$.

[†] Extracted values of γ_L and n_γ for $J''=16$ are 0.041(12) and -0.00(27), which are out of the trend. Therefore, these values are replaced with the expected values from the polynomial equation 9 due to the weakness of the lines.

[‡] The extracted values of γ_L and n_γ for $J''=16$ are 0.008(6) and -1.50(66), which are out of the trend. Therefore, these values are replaced with the expected values from the polynomial equation 9 due to the weakness of the lines.

7. Reference

References

- [1] V. A. Krasnopolsky, J. P. Maillard, T. C. Owen, Detection of methane in the martian atmosphere: evidence for life?, *Icarus* 172 (2) (2004) 537–547, ISSN 0019-1035.
- [2] J. R. Lyons, C. Manning, F. Nimmo, Formation of methane on Mars by fluid-rock interaction in the crust, *GRL* 32 L13201.
- [3] G. S. Orton, J. I. Moses, L. N. Fletcher, A. K. Mainzer, D. Hines, H. B. Hammel, J. Martin-Torres, M. Burgdorf, C. Merlet, M. R. Line, Mid-infrared spectroscopy of Uranus from the Spitzer infrared spectrometer: 2. Determination of the mean composition of the upper troposphere and stratosphere, *Icarus* 243 (2014) 471–493, ISSN 0019-1035.
- [4] G. S. Orton, L. N. Fletcher, J. I. Moses, A. K. Mainzer, D. Hines, H. B. Hammel, F. J. Martin-Torres, M. Burgdorf, C. Merlet, M. R. Line, Mid-infrared spectroscopy of Uranus from the Spitzer Infrared Spectrometer: 1. Determination of the mean temperature structure of the upper troposphere and stratosphere, *Icarus* 243 (2014) 494–513, ISSN 0019-1035.
- [5] S. K. Atreya, P. R. Mahaffy, H. B. Niemann, M. H. Wong, T. C. Owen, Composition and origin of the atmosphere of Jupiter - An update, and implications for the extrasolar giant planets, *Planetary and Space Science* 51 (2) (2003) 105–112, ISSN 00320633.
- [6] K. Lodders, *Exoplanet Chemistry*, 157, 2010.
- [7] M. S. Marley, T. D. Robinson, On the Cool Side: Modeling the Atmospheres of Brown Dwarfs and Giant Planets, *ARAA* 53 (2015) 279–323, ISSN 0066-4146.
- [8] J. J. Fortney, On the Carbon-to-oxygen Ratio Measurement in nearby Sun-like Stars: Implications for Planet Formation and the Determination of Stellar Abundances, *ApJL* 747 L27.
- [9] O. Venot, M. Agúndez, F. Selsis, M. Tessenyi, N. Iro, The atmospheric chemistry of the warm Neptune GJ 3470b: Influence of metallicity and temperature on the CH₄/CO ratio, *A&A* 562 (2014) A51, ISSN 0004-6361.
- [10] L. Kreidberg, M. R. Line, D. Thorngren, C. V. Morley, K. B. Stevenson, Water, High-altitude Condensates, and Possible Methane Depletion in the Atmosphere of the Warm Super-Neptune WASP-107b, *AJ* 858 (1) (2018) L6, ISSN 2041-8213.
- [11] A. J. Burgasser, T. R. Geballe, S. K. Leggett, J. D. Kirkpatrick, D. A. Golimowski, A Unified Near-Infrared Spectral Classification Scheme for T Dwarfs, *AJ* 637 (2) (2006) 1067–1093, ISSN 0004-637X.
- [12] M. R. Line, G. Vasisht, P. Chen, D. Angerhausen, Y. L. Yung, Thermochemical and Photochemical Kinetics in Cooler Hydrogen-dominated Extrasolar Planets: A Methane-poor GJ436b?, *ApJ* 738 32.
- [13] L. Kreidberg, M. R. Line, D. Thorngren, C. V. Morley, K. B. Stevenson, Water, High-altitude Condensates, and Possible Methane Depletion in the Atmosphere of the Warm Super-Neptune WASP-107b, *APJL* 858 L6.
- [14] M. R. Swain, P. Deroo, C. A. Griffith, G. Tinetti, A. Thatte, G. Vasisht, P. Chen, J. Bouwman, I. J. Crossfield, D. Angerhausen, C. Afonso, T. Henning, A ground-based near-infrared emission spectrum of the exoplanet HD189733b, *Nature* 463 (2010) 637–639.
- [15] J.-M. Désert, A. Lecavelier des Etangs, G. Hébrard, D. K. Sing, D. Ehrenreich, R. Ferlet, A. Vidal-Madjar, Search for Carbon Monoxide in the Atmosphere of the Transiting Exoplanet HD 189733b, *ApJ* 699 (2009) 478–485.
- [16] J. Wang, D. Mawet, J. J. Fortney, C. Hood, C. V. Morley, B. Benneke, Detecting Water in the Atmosphere of HR 8799 c with L-band High-dispersion Spectroscopy Aided by Adaptive Optics, *AJ* 156 272.
- [17] J. I. Moses, M. R. Line, C. Visscher, M. R. Richardson, N. Nettelmann, J. J. Fortney, T. S. Barman,

- K. B. Stevenson, N. Madhusudhan, Compositional Diversity in the Atmospheres of Hot Neptunes, with Application to GJ436b, *ApJ* 777 (1) (2013) 34, ISSN 0004-637X.
- [18] M. Brogi, M. R. Line, Retrieving Temperatures and Abundances of Exoplanet Atmospheres with High-resolution Cross-correlation Spectroscopy, *AJ* 157 (3) (2019) 114.
- [19] R. S. Freedman, J. Lustig-Yaeger, J. J. Fortney, R. E. Lupu, M. S. Marley, K. Lodders, Gaseous mean opacities for giant planet and ultracool dwarf atmospheres over a range of metallicities and temperatures, *ApJS* 214 (2), ISSN 00670049.
- [20] E. Gharib-Nezhad, M. R. Line, The Influence of H₂O Pressure Broadening in High-metallicity Exoplanet Atmospheres, *ApJ* 872 (1) (2019) 27.
- [21] J. J. Fortney, T. D. Robinson, S. Domagal-Goldman, A. D. Del Genio, I. E. Gordon, E. Gharib-Nezhad, et. al., The Need for Laboratory Measurements and Ab Initio Studies to Aid Understanding of Exoplanetary Atmospheres, arXiv e-prints .
- [22] P. Bernath, *Spectra of Atoms and Molecules*, Oxford University Press, 2 edn., ISBN 9780195177596, 2005.
- [23] S. Albert, S. Bauerecker, V. Boudon, L. R. Brown, J.-P. Champion, M. Loëte, A. Nikitin, M. Quack, Global analysis of the high resolution infrared spectrum of methane ¹²CH₄ in the region from 0 to 4800 cm⁻¹, *Chemical Physics* 356 (2009) 131–146.
- [24] A. Campargue, O. Leshchishina, L. Wang, D. Mondelain, S. Kassi, The WKLMC empirical line lists (58527919cm⁻¹) for methane between 80K and 296K: Final lists for atmospheric and planetary applications, *JMS* 291 (2013) 16–22, ISSN 0022-2852.
- [25] A. Wong, P. F. Bernath, M. Rey, A. V. Nikitin, V. G. Tyuterev, Atlas of Experimental and Theoretical High-temperature Methane Cross Sections from T=295 to 1000 K in the Near-infrared, *ApJS* 240 4.
- [26] R. J. Hargreaves, P. F. Bernath, J. Bailey, M. Dulick, Empirical Line Lists and Absorption Cross Section for Methane at High Temperatures, *ApJ* 813 (1) (2015) 12, ISSN 1538-4357.
- [27] R. Nassar, P. Bernath, Hot methane spectra for astrophysical applications, *JQSRT* 82 (1-4) (2003) 279–292, ISSN 00224073.
- [28] M.-Y. Perrin, A. Soufiani, Approximate radiative properties of methane at high temperature, *JQSRT* 103 (1) (2007) 3–13, ISSN 00224073.
- [29] R. J. Hargreaves, C. A. Beale, L. Michaux, M. Irfan, P. F. Bernath, Hot Methane Line Lists for Exoplanet and Brown Dwarf Atmospheres, *ApJ* 757 (1) (2012) 46, ISSN 0004-637X.
- [30] J. Thiévin, R. Georges, S. Carles, A. Benidar, B. Rowe, J.-P. Champion, High-temperature emission spectroscopy of methane, *JQSRT* 109 (11) (2008) 2027–2036, ISSN 00224073.
- [31] Y. A. Ba, C. Wenger, R. Surlleau, V. Boudon, L. Daumont, D. A. Bonhommeau, V. G. Tyuterev, M.-L. Dubernet, MeCaSDa and ECaSDa: Methane and ethene calculated spectroscopic databases for the virtual atomic and molecular data centre, *JQSRT* 130 (2013) 62–68, ISSN 0022-4073.
- [32] A. Nikitin, O. Lyulin, S. Mikhailenko, V. Perevalov, N. Filippov, I. Grigoriev, I. Morino, Y. Yoshida, T. Matsunaga, GOSAT-2014 methane spectral line list, *JQSRT* 154 (2015) 63–71, ISSN 00224073.
- [33] M. Rey, A. V. Nikitin, V. G. Tyuterev, Accurate Theoretical Methane Line Lists in the Infrared up to 3000 K and Quasi-continuum Absorption/Emission Modeling for Astrophysical Applications, *ApJ* 847 (2) (2017) 105, ISSN 1538-4357.
- [34] M. Rey, A. V. Nikitin, B. Bézard, P. Rannou, A. Coustenis, V. G. Tyuterev, New accurate theoretical line lists of ¹²CH₄ and ¹³CH₄ in the 013400cm⁻¹ range: Application to the modeling of methane absorption in Titan’s atmosphere, *Icarus* 303 (2018) 114–130, ISSN 0019-1035.

- [35] A. S. Pine, Self-, N₂, O₂, H₂, Ar, and He broadening in the ν_3 band Q branch of CH₄, JCP 97 (1992) 773–785.
- [36] A. Pine, T. Gabard, Multispectrum fits for line mixing in the ν_3 band Q branch of methane, JMS 217 (1) (2003) 105–114, ISSN 0022-2852.
- [37] K. Fox, D. E. Jennings, Measurements of nitrogen-, hydrogen- and helium-broadened widths of methane lines at 90309120 cm⁻¹, JQSRT 33 (3) (1985) 275–280, ISSN 0022-4073.
- [38] K. Fox, D. E. Jennings, E. A. Stern, R. Hunnard, Measurements of argon-, helium-, hydrogen-, and nitrogen-broadened widths of methane lines near 9000 cm⁻¹, JQSRT 39 (6) (1988) 473–476, ISSN 0022-4073.
- [39] J.-M. Hartmann, H. Tran, R. Armante, C. Boulet, A. Campargue, F. Forget, L. Gianfrani, I. Gordon, S. Guerlet, M. Gustafsson, J. T. Hodges, S. Kassi, D. Lisak, F. Thibault, G. C. Toon, Recent advances in collisional effects on spectra of molecular gases and their practical consequences, JQSRT 213 (2018) 178–227, ISSN 0022-4073.
- [40] P. W. Anderson, Pressure Broadening in the Microwave and Infra-Red Regions, Phys. Rev. 76 (1949) 647–661.
- [41] B. S. Frost, A theory of microwave lineshifts, Journal of Physics B: Atomic and Molecular Physics 9 (6) (1976) 1001–1020.
- [42] G. D. T. Tejwani, P. Varanasi, Calculation of Collision-Broadened Linewidths in the Infrared Bands of Methane, JCP 55 (1971) 1075–1083.
- [43] V. Devi, B. Fridovich, D. Snyder, G. Jones, P. P. Das, Tunable diode laser measurements of intensities and Lorentz broadening coefficients of lines in the 2 band of 12CH₄, JQSRT 29 (1) (1983) 45 – 47, ISSN 0022-4073.
- [44] T. Gabard, Calculated line broadening parameters for methane perturbed by diatomic molecules, JMS 291 (2013) 61 – 68, ISSN 0022-2852.
- [45] S. P. Neshyba, R. Lynch, R. Gamache, T. Gabard, J. Champion, Pressureinduced widths and shifts for the 3 band of methane, JCP 101 (11) (1994) 9412–9421.
- [46] P. Varanasi, Air-broadened line widths of methane at atmospheric temperatures, JQSRT 15 (3) (1975) 281, ISSN 0022-4073.
- [47] M. Smith, C. Rinsland, V. Devi, D. Benner, Temperature dependence of broadening and shifts of methane lines in the ν_4 band, Spectrochimica Acta Part A: Molecular Spectroscopy 48 (9) (1992) 1257–1272, ISSN 0584-8539.
- [48] L. Brown, J. Margolis, J. Champion, J. Hilico, J. Jouvard, M. Loete, C. Chackerian, G. Tarrago, D. Benner, Methane and its isotopes: Current status and prospects for improvement, JQSRT 48 (5) (1992) 617 – 628, ISSN 0022-4073, special Issue Conference on Molecular Spectroscopic Databases.
- [49] C. Guret, M. Daroux, F. Billaud, Methane pyrolysis: thermodynamics, Chemical Engineering Science 52 (5) (1997) 815 – 827, ISSN 0009-2509.
- [50] I. Gordon, L. Rothman, C. Hill, R. Kochanov, Y. Tan, P. Bernath, M. Birk, V. Boudon, A. Campargue, K. Chance, B. Drouin, J.-M. Flaud, R. Gamache, J. Hodges, D. Jacquemart, V. Perevalov, A. Perrin, K. Shine, M.-A. Smith, J. Tennyson, G. Toon, H. Tran, V. Tyuterev, A. Barbe, A. Császár, V. Devi, T. Furtenbacher, J. Harrison, J.-M. Hartmann, A. Jolly, T. Johnson, T. Karman, I. Kleiner, A. Kyuberis, J. Loos, O. Lyulin, S. Massie, S. Mikhailenko, N. Moazzen-Ahmadi, H. Müller, O. Naumenko, A. Nikitin, O. Polyansky, M. Rey, M. Rotger, S. Sharpe, K. Sung, E. Starikova, S. Tashkun, J. V. Auwera, G. Wagner, J. Wilzewski, P. Wcisło, S. Yu, E. Zak, The HITRAN2016 molecular spectroscopic database, JQSRT 203 (2017) 3–69, ISSN 00224073.
- [51] L. Brown, K. Sung, D. Benner, V. Devi, V. Boudon, T. Gabard, C. Wenger, A. Campargue, O. Leshchishina, S. Kassi, D. Mondelain, L. Wang, L. Daumont, L. Régalia, M. Rey, X. Thomas, V. G. Tyuterev, O. Lyulin, A. Nikitin, H. Niederer,

- S. Albert, S. Bauerecker, M. Quack, J. O'Brien, I. Gordon, L. Rothman, H. Sasada, A. Coustenis, M. Smith, T. Carrington, X.-G. Wang, A. Mantz, P. Spickler, Methane line parameters in the HITRAN2012 database, *JQSRT* 130 (2013) 201–219, ISSN 00224073.
- [52] R. Bretzlaff, T. Bahder, Apodization effects in Fourier transform infrared difference spectra, *Revue de Physique Appliquée* 21 (12) (1986) 833–844, ISSN 0035-1687.
- [53] R. L. Burden, J. D. Faires, A. M. Burden, Numerical analysis, Cengage Learning US, 9th edn., ISBN 9781305253667, 2011.
- [54] J. Buldyreva, N. Lavrentieva, V. Starikov, Collisional Line Broadening and Shifting of Atmospheric Gases: a Practical Guide for Line Shape Modelling by Current Semi-Classical Approaches, World Scientific Publishing Co, 2011.
- [55] W. Jin, S. Murray, D. Pinchbeck, G. Stewart, B. Culshaw, Absorption measurement of methane gas with a broadband light source and interferometric signal processing, *Optics Letters* 18 (16) (1993) 1364, ISSN 0146-9592.
- [56] R. Kochanov, I. Gordon, L. Rothman, P. WcisÅo, C. Hill, J. Wilzewski, HITRAN Application Programming Interface (HAPI): A comprehensive approach to working with spectroscopic data, *Journal of Quantitative Spectroscopy and Radiative Transfer* 177 (2016) 15 – 30, ISSN 0022-4073, xVIIIth Symposium on High Resolution Molecular Spectroscopy (HighRus-2015), Tomsk, Russia.
- [57] R. S. Freedman, M. S. Marley, K. Lodders, Line and Mean Opacities for Ultracool Dwarfs and Extrasolar Planets, *ApJS* 174 (2008) 504–513.
- [58] Yurchenko, Sergei N., Al-Refaie, Ahmed F., Tenynson, Jonathan, EXOCROSS: a general program for generating spectra from molecular line lists, *A&A* 614 (2018) A131.
- [59] D. Robert, J. Bonamy, Short range force effects in semiclassical molecular line broadening calculations, *Journal de Physique* 40 (10) (1979) 923–943.
- [60] L. N. Smith, D. Secrest, Close coupling and coupled state calculations of argon scattering from normal methane, *JCP* 74 (7) (1981) 3882–3897.
- [61] M. Baranger, Simplified Quantum-Mechanical Theory of Pressure Broadening, *Physical Review* 111 (2) (1958) 481–493, ISSN 0031-899X.
- [62] J. Lyons, H. Herde, G. Stark, D. Blackie, J. Pickering, N. de Oliveira, VUV pressure-broadening in sulfur dioxide, *JQSRT* 210 (2018) 156 – 164, ISSN 0022-4073.
- [63] R. R. Gamache, B. Vispoel, On the temperature dependence of half-widths and line shifts for molecular transitions in the microwave and infrared regions, *JQSRT* 217 (2018) 440 – 452, ISSN 0022-4073.
- [64] C. E. Keffer, C. P. Conner, W. Smith, Pressure broadening of methane lines in the 6190Å and 6825Å bands at room and low temperatures, *JQSRT* 35 (6) (1986) 495–499, ISSN 0022-4073.
- [65] P. Varanasi, Temperature Dependence of Strengths, Widths and Shifts of CH₄ at Planetary Atmospheric Temperatures, *BAAS* 21 (1989) 961.
- [66] P. Varanasi, S. Chudamani, Measurements of collision-broadened line widths in the nu₄-fundamental band of (C-12)H₄ at low temperatures, *JQSRT* 41 (1989) 335–343.
- [67] P. Varanasi, S. Chudamani, The temperature dependence of lineshifts, linewidths and line intensities of methane at low temperatures, *JQSRT* 43 (1) (1990) 1–11, ISSN 0022-4073.
- [68] V. Devi, D. Benner, M. Smith, C. Rinsland, Temperature dependence of Lorentz air-broadening and pressure-shift coefficients of ¹²CH₄ lines in the 2.3-μm spectral region, *JQSRT* 51 (3) (1994) 439–465, ISSN 0022-4073.
- [69] D. Mondelain, S. Payan, W. Deng, C. Camy-Peyret, D. Hurtmans, A. W. Mantz, Measurement of the temperature dependence of line mixing and pressure broadening parameters between 296 and 90K in the ν₃ band of ¹²CH₄ and their influence on atmospheric methane retrievals, *JMS* 244 (2) (2007) 130–137, ISSN 0022-2852.

- [70] V. Markov, Temperature Dependence of Self-Induced Pressure Broadening and Shift of the 643-550 Line of the Water Molecule, *JMS* 164 (1) (1994) 233 – 238, ISSN 0022-2852.
- [71] G. Baldacchini, G. Buffa, F. D'Amato, F. Pelagalli, O. Tarrini, Variations in the sign of the pressure-induced lineshifts in the 2 band of ammonia with temperature, *JQSRT* 55 (6) (1996) 741 – 743, ISSN 0022-4073.
- [72] A. Pine, Speed-dependent Line Mixing in the ν_3 Band *Q* Branch of Methane, *JQSRT* 224 (2019) 62 – 77, ISSN 0022-4073.
- [73] E. Es-sebbar, A. Farooq, Intensities, Broadening and Narrowing Parameters in the ν_3 band of Methane, *JQSRT* 149 (2014) 241 – 252, ISSN 0022-4073.
- [74] M. Smith, D. C. Benner, A. Predoi-Cross, V. M. Devi, Multispectrum Analysis of $^{12}\text{CH}_4$ in the ν_4 band, *JQSRT* 110 (9-10) (2009) 639–653, ISSN 00224073.
- [75] A. S. Pine, N_2 and Ar broadening and line mixing in the P and R branches of the ν_3 band of CH_4 , *JQSRT* 57 (1997) 157–176.